20th Australasian Fluid Mechanics Conference
Perth, Australia
5-8 December 2016

Air-Water Flow in Hydraulic Jumps on Macro-Roughness

S. Felder[1] and H. Chanson[2]

[1]Water Research Laboratory, School of Civil and Environmental Engineering,
UNSW Australia, Sydney, New South Wales, 2052, Australia

[2]School of Civil Engineering, The University of Queensland, Brisbane, Queensland, 4072, Australia

Abstract

Hydraulic jumps are highly complex three dimensional flows with strong energy dissipation and air bubble entrainment associated with intense mixing. To date turbulence and air-water flow observations in hydraulic jumps have been limited to smooth rectangular channels. Herein novel experiments were conducted on a channel with bed macro roughness to characterise the effect of boundary roughness on the air-water flow properties. The results showed distinctive differences including a reduction in hydraulic jump length and upward shift of the roller toe for a rough bed jump. The air-water flow profiles were comparable with larger aeration downstream of the jump toe for the rough bed and a reduction in aeration and interfacial velocity compared to a smooth bed flow towards the downstream end of the jump. The present study highlighted the potential to use macro roughness boundaries to manipulate the flow performance and the re-aeration capabilities of turbulent hydraulic jumps.

Introduction

Hydraulic jumps occur in natural waterways, open channels and canals as well as downstream of man-made hydraulic structures when fast flowing supercritical flow transitions into subcritical flows [2,3]. The transition is sudden, extremely turbulent and associated with energy dissipation, air entrainment, large-scale turbulence, spray, splashing, and surface waves (Fig. 1). Figure 1 illustrates a hydraulic jump in a laboratory channel highlighting the jump characteristics of high turbulence and strong air bubble entrainment. The flow turbulence in hydraulic jumps is extremely complicated and it remains a challenge to engineers, scientists and researchers [6]. Basic features of jumps with a breaking roller are the development of large-scale vortices, the air bubble entrapment at the jump toe, the interfacial aeration/de-aeration at the roller upper free-surface and the interactions between entrained bubbles and coherent turbulent structures in the jump roller (Fig. 1). To date most research has focused upon hydraulic jumps in smooth rectangular channels [1,14,15,16].

The effects of bed roughness on hydraulic jumps were investigated (a) in terms of the impact of baffles in stilling basins [4] and (b) with uniformly distributed roughness. On uniform rough bed, most investigations focused on simple free-surface measurements to identify the conjugate depth ratio: i.e., the ratio of downstream to upstream depths [10,13]. Bed roughness leads to loss of momentum through the friction force F_{fric} on the channel bed for macro-rough bed configurations. For a rectangular horizontal channel, the application of the continuity and momentum principles in an integral form provide the hydraulic jump equation:

$$Fr_1^2 = \frac{1}{2} \times \frac{d_2}{d_1} \times \left(\left(1 + \frac{d_2}{d_1}\right) + \frac{1}{\frac{d_2}{d_1} - 1} \times \frac{F_{fric}}{\rho \times g \times B \times d_1^2} \right) \quad (1)$$

where Fr_1 is the upstream Froude number, d_1 and d_2 are the conjugate flow depths measured upstream and downstream of the hydraulic jump roller respectively, ρ is the density of the fluid, g is the gravity acceleration and B is the channel width.

Recently [12] used a single-tip phase-detection probe to measure the conjugate depth taking into account any pre-aeration effect upstream of the jump and flow aeration downstream of the jump. While this study highlighted the relevance of aeration on the conjugate depth relationship, no study considered the bed roughness effects on the microscopic air-water flows in hydraulic jumps. Herein, the present study systematically investigated the effects of macro-channel bed roughness upon the basic two-phase flow patterns and air-water flow properties in hydraulic jumps.

Figure 1. Laboratory hydraulic jump on smooth bed: Fr_1 = 4.5; Re = 1.8×10^5; B = 0.5 m; d_1 = 0.055 m; x_1 = 1.25 m; flow from right to left

Experimental Facility and Instrumentation

Experiments were conducted in a large experimental facility with rectangular test section of 3.2 m length, 0.5 m width and 0.41 m height, consisting of a horizontal high-density polyethylene (HDPE) bed and glass sidewalls [8]. A constant flow rate was supplied from an upstream header tank through a vertical sluice gate equipped with a rounding (Ø = 0.3 m). At the downstream end of the test section, an adjustable sharp crested weir controlled the location of the hydraulic jump toe, set herein at x_1 = 1 m downstream of the sluice gate for all flow conditions. Experiments were conducted for a range of discharges $0.012 < Q_w < 0.106$ m^3/s. Three different sluice gate openings (h = 20 mm, 36 mm and 52 mm) were tested to achieve a broad range of Reynolds numbers $3.3 \times 10^4 < Re < 1.5 \times 10^5$. The experimental flow conditions comprised upstream Froude numbers between $1.5 < Fr_1 < 6.5$.

The roughness effects on hydraulic jumps were tested using two different bed roughness configurations. The first configuration

was the original un-modified smooth reference, a configuration extensively researched in recent years [5,11,14,15]. The other setup comprised a bed roughness configuration consisting of industrial rubber mats installed over the full length of the channel bed including in the header tank and underneath the sluice gate (Fig. 2). The rubber mat resulted in small continuous gaps between the HDPE invert and rubber mat floor. The total thickness of the rubber mat from the HDPE bed to the top of the mat was 25.5 mm. The top of the rubber mat was defined as the zero position for the vertical elevations and visual observations confirmed little contribution of the underlying gaps to the overall flow rate. [9] quantified the characteristics of the rubber mat during detailed open channel flow experiments, leading to an equivalent sand roughness height k_s = 12 mm.

Figure 2. Bed roughness configuration; Note the sluice gate in the background

Air-water flow measurements were conducted with a dual-tip phase-detection intrusive probe manufactured at UNSW's Water Research Laboratory. The conductivity probe had two tips separated in longitudinal and transverse directions by Δx = 7.9 mm and Δz = 1.0 mm respectively. Each needle sensor consisted of an inner Platinum wire (inner electrode) which was shielded with an insulant from the surrounding metal tube (outer electrode). The diameters of the electrodes were Ø = 0.125 mm and Ø = 0.5 mm respectively. The leading tip sensor was positioned in channel centre line and shifted vertically with a Mitutoyo^{TM} digimatic scale. The phase-detection probe tips were sampled simultaneously with an acquisition card NI USB-6251 BNC connected to a computer. Both sensors were sampled for 45 s at 20 kHz per sensor at each location following [7].

The raw Voltage signals of the leading tip were post processed based upon a single-threshold technique providing the time averaged local void fraction C and the bubble count rate F. The cross-correlation of the simultaneously sampled leading and trailing tips yielded the time-averaged interfacial velocity V. More details about the signal processing can be found in [7]. The conductivity probe was not only used for measurement of air-water flow properties within the hydraulic jump roller, but also to determine the upstream flow depth d_1 due to the pre-aeration of the flow using the equivalent clear water flow depth d since:

$$d = \int_{y=0}^{Y_{90}} (1-C) \times dy \quad (2)$$

where Y_{90} is the characteristic depth where C = 0.9. In addition to the air-water flow instrumentation, a pointer gauge was used to record non-aerated flow depths upstream and downstream of the hydraulic jump. Detailed documentation of the flow patterns was conducted with digital cameras Canon^{TM} DOS 450D and Pentax^{TM} K-3.

For a range of flow conditions, detailed air-water flow experiments were conducted (Table 1). Table 1 summarises the experimental conditions of the present study including the gate opening h, the Froude and Reynolds numbers and the bed roughness configuration.

Configuration	h [mm]	Q_w [m^3/s]	d_1 [mm]	Fr_1 [-]	Re [-]
Smooth	36	0.054	36	5.1	1.1×10^5
Rough	20	0.045	34	4.6	9.0×10^4
		0.065	34	6.5	1.3×10^5
	36	0.071	48	4.3	1.4×10^5
		0.083	45	5.5	1.6×10^5
	52	0.103	63	4.2	2.0×10^5

Table 1. Experimental flow conditions for air-water flow experiments with double-tip conductivity probe in the present study.

Flow Patterns in Hydraulic Jumps on Macro-roughness

The visual observations showed a variety of hydraulic jump patterns on the rough bed (Fig. 3). The jumps were classified as undular jumps without air entrainment, undular jumps with small air entrainment, hydraulic jumps with small roller and wavy surface downstream and hydraulic jumps with distinct jump toe roller, with increasing Froude number. For all flow conditions, the free-surface was rough with small ripples present in both super- and sub-critical flow regions in particular for flow regions with small flow depths (e.g. supercritical flow region upstream of jump toe).

(A) Hydraulic jump with small roller and wavy free-surface: Fr_1 = 2.8; Q_w = 0.03 m^3/s; Re = 6.0×10^4; h = 20 mm (flow from top to bottom)

(B) Jump with stable roller and pre-aerated flow: Fr_1 = 4.3; Q_w = 0.058 m^3/s; Re = 1.2×10^5; h = 20 mm (flow from bottom to top)

Figure 3. Flow patterns on the hydraulic jump with rough bed

For the smallest Froude numbers, an undular hydraulic jump without air entrainment was observed independently of the gate opening for Froude numbers $Fr_1 \leq 2.2$. The flow patterns showed a three dimensional free-surface profile with instable undulations, oscillating in both longitudinal and transverse directions. Within the central section of the undular jump, distinct standing waves were observed with several troughs and peaks. For $2.2 < Fr_1 \leq 2.6$, undular hydraulic jumps with air entrainment were observed. These jumps were similar in appearance to the non-aerated undular hydraulic jumps, albeit with stronger free-surface fluctuations and standing waves. A key feature was the entrainment of air bubbles at the first undular wave crest downstream of the jump toe and to a lesser extent at the following wave crests.

With an increasing Froude number, a roller formed at the jump toe. For $2.7 \leq Fr_1 \leq 2.9$, the roller formation at the jump toe was unstable resulting in secondary undulations of the free-surface further downstream (Fig. 3A). The roller length ranged between $0.15 \leq L_r/d_1 \leq 6.7$, and the air entrainment region length between $3.9 \leq L_a/d_1 \leq 27$. The jump was affected by the upstream flow motion, resulting in less stable roller formation for the smallest

gate opening. Figure 3A illustrates the instable hydraulic jump flow pattern.

For $Fr_1 \geq 3.0$, the hydraulic jump had a marked roller with strong turbulence downstream of the jump toe (Fig. 3B). Upstream of the jump, the supercritical inflow was characterised by strong free-surface ripples which increased with decreasing inflow depth. For the smallest gate opening (h = 20 mm), the flow became pre-aerated for the largest flow rates (Fig. 3B). For all flow conditions, the jump toe fluctuated in longitudinal direction, in a manner similar to known features of hydraulic jumps on smooth bed [5,14]. While the bed roughness appeared to stabilise the overall longitudinal position of the jump, fast fluctuating movement of the jump toe were observed. Although the overall appearance of the jumps with stable roller was similar to hydraulic jumps on smooth bed, a distinctive difference was the large-scale vortical structures downstream of the jump toe. For the two largest gate openings, the jump toe was shifted upwards, towards the surface, resulting in a clear water flow region below the jump roller. The occurrence of this clear water flow region resulted in a distinctive formation of vortex street downstream of the jump toe, with periodic air bubble vortex shedding into the clear water core region under the jump. Interactions between the clear water boundary layer and the vortex shedding led to the formation of large scale eddies within the flow consisting of tube-like vortical structures that were advected downstream. The air entrainment length in jumps on rough bed appeared to be smaller than that in a comparable hydraulic jump on smooth bed. More detailed description and illustrations can be found in [8].

Flow Properties in Hydraulic Jumps with Rough Bed

A comparative analysis of air-water flow properties was conducted for experimental data with comparable Froude and Reynolds numbers (Table 1). In Figure 4, typical air-water flow properties are shown in dimensionless form as function of the dimensionless elevation above channel bed y/d_1, including the void fraction (Fig. 4A), the bubble count rate (Fig. 4B) and the interfacial velocity (Fig. 4C). Overall the present data set highlighted a few key differences between the rough bed configuration and smooth bed jump data.

The void fraction distributions had similar shapes independently of the bed roughness. In the turbulent shear region, a local maximum void fraction C_{max} was observed, while a local minimum C* was found at the boundary between the shear region and the recirculation region above. Close to the invert, the void fraction tended to zero. In the free-surface region the void fraction increased sharply with increasing elevation towards unity (Fig. 4A). The distributions of void fraction were almost identical immediately downstream of the jump toe ($x-x_1/d_1 \leq 3.2$), for both bed configurations, although the minimum void fraction C* tended to be larger on the rough bed. The strongest difference was observed in terms of shape within the turbulent shear region at the downstream end of the roller. In the smooth bed hydraulic jump, a clearly distinct shear layer region was observed ($x-x_1/d_1 = 15.3$) while no clear shear layer region was observed for the void fraction distributions in the rough bed hydraulic jump ($x-x_1/d_1 = 16.8$) (Fig. 4A). The turbulent shear region was shifted upwards on the rough bed, associated with a decrease in hydraulic jump roller length.

The analyses of bubble count rate distributions revealed a distinctive effect of bed macro-roughness (Fig. 4B), albeit that the present comparative analysis did not achieve exact similitude in terms of both Froude and Reynolds numbers. The comparison between smooth and rough bed showed a similar shape of bubble count rate distributions, with a distinctive maximum in the shear layer and a secondary peak in the recirculation region about C ~ 50% (Fig. 4B). While the bubble count rate was slightly higher on the rough channel bed at the start of the roller, the bubble count rates were larger on the smooth bed jump further downstream. The largest differences were observed towards the downstream part of the roller, and this was consistent with an upward shift of the hydraulic jump roller on the rough invert. This finding was consistent with visual observations of a shorter roller length and the existence of clear water region underneath the jump on the rough bed.

The comparison of interfacial velocities showed overall similar shapes in velocity distributions for both bed configurations including maximum velocities in the shear layer close to the jump toe and negative velocities in the recirculation region (Fig. 4C). Clear differences were observed at the downstream end of the hydraulic jump where smaller velocities were observed in the region close to the rough bed. At the downstream end, the velocity distributions were more uniform on the rough bed. The bed roughness resulted in both a reduction in flow velocity and reduction in recirculation motions. This finding was in agreement with the observation of the clear water region underneath the roller and an upwards shift of the hydraulic jump on rough bed.

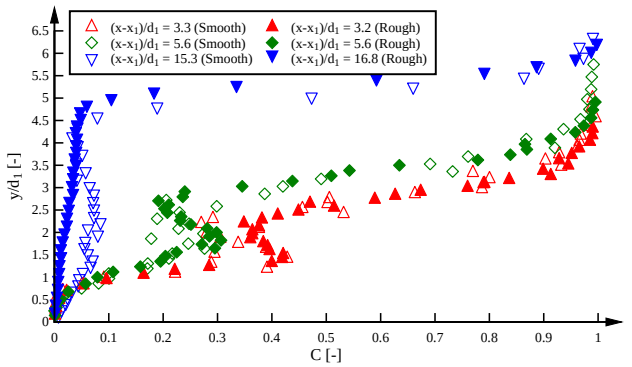

(A) Void fraction distributions

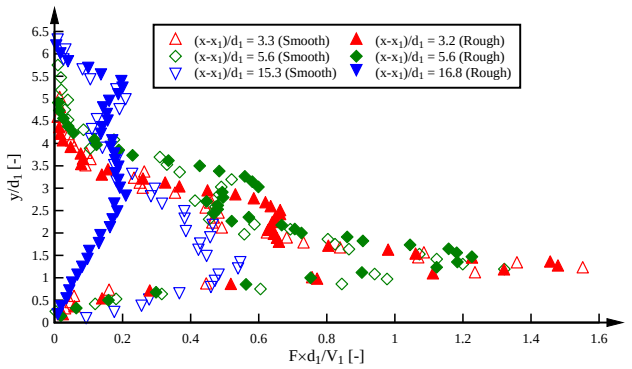

(B) Bubble count rate distributions

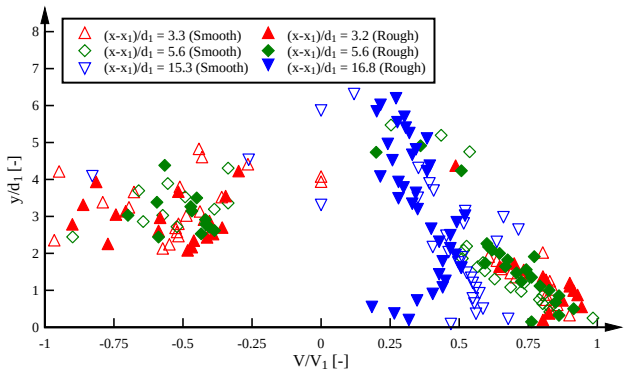

(C) Interfacial velocity distribution

Figure 4. Basic air-water flow properties in hydraulic jumps with different bed roughness: Rough bed: $Fr_1 = 4.6$, $Re = 9.0 \times 10^4$, h = 20 mm; Smooth bed: $Fr_1 = 5.1$, $Re = 1.1 \times 10^5$, h = 36 mm

The comparative analysis was extended to a range of characteristic air-water flow parameters [8]. Figure 5 illustrates the longitudinal distributions of local maximum void fraction C_{max} and dimensionless maximum bubble count rate in a cross-section F_{max}. Both rough and smooth bed data are illustrated as functions of the dimensionless distance from the jump toe. The data are compared to previous smooth bed jump data with similar Froude number [6,11,14,15]. A marked difference was observed between the rough and smooth bed data for a comparable Froude number. The rough bed induced larger maximum void fractions at all locations within the hydraulic jump. The difference increased with increasing Froude number. For some rough bed data, the flow was pre-aerated and this might have contributed to the local increased aeration.

A comparison in terms of maximum bubble count rate indicated significantly larger maximum bubble count rates F_{max} at the start of the roller for the rough bed configuration. That is, within the experimental conditions, the maximum bubble count rate increased with increasing bed roughness. This trend vanished towards comparable maximum bubble frequencies for all channel bed configurations at the roller's downstream end. Similar results were also observed for several other characteristic air-water flow properties including the local maximum bubble count rate F_{sec} in the recirculation region [8].

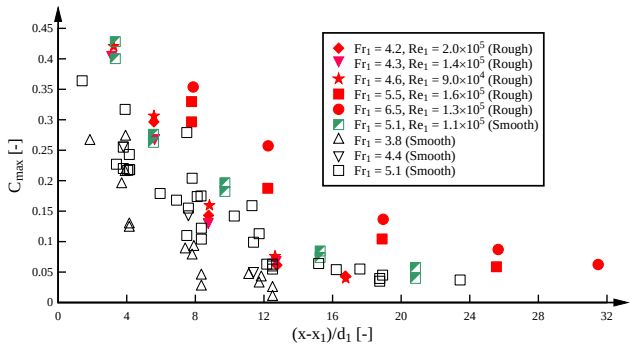

(A) Maximum void fraction in a cross-section

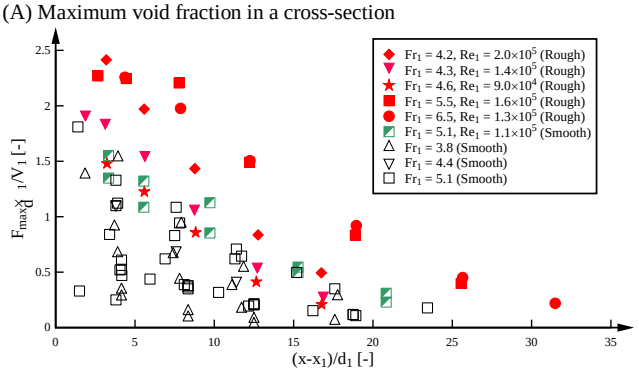

(B) Maximum bubble count rate in a cross-section

Figure 5. Basic air-water flow properties in hydraulic jumps with rough bed - comparison with smooth bed data in previous studies [6,12,15,16] – coloured symbols: present data

Conclusion

New experiments were conducted in hydraulic jumps in a channel with uniformly distributed bed macro-roughness. Two-phase flow measurements were performed using phase-detection intrusive sensors. The study focused on the air-water turbulent flow patterns and air-water flow characteristics. The results were compared to experimental data of hydraulic jumps on smooth channel bed, with similar Froude and Reynolds numbers. The comparative analyses identified significant differences in terms of flow patterns, including some pre-aeration of the supercritical inflow, an upward shift of the mixing zone, a reduction of jump length and a clear water flow region underneath the jump on rough bed. Overall the distributions of air-water flow properties were qualitatively comparable for rough and smooth bed hydraulic jumps, albeit quantitatively different. Distinctive effects of the bed roughness included an increase in bubble count rate and void fractions in the region close to the jump toe, and an upward change next to the roller toe. In the second half of the hydraulic jump roller, the rough bed induced a lesser aeration of the shear layer region and a reduction in flow velocity. The present study highlighted the potential to improve existing stilling basin designs and develop non-standard designs using turbulent flow manipulations and boundary condition changes.

References

[1] Babb, A.F., & Aus, H.C., Measurements of Air in Flowing Water. *Jl. Hyd. Div., ASCE*, 1981, **107**, 1615-1630.

[2] Bakhmeteff, B.A., *Hydraulics of Open Channels*. McGraw-Hill, New York, 329 pages.

[3] Bélanger, J.B., *Notes sur l'Hydraulique*. Ecole Royale des Ponts et Chaussées, Paris, 1841, 223 pages (in French).

[4] Bradley, J.N., & Peterka, A.J., The Hydraulic Design of Stilling Basins: Hydraulic Jumps on a Horizontal Apron (Basin I). *Jl. Hyd. Div., ASCE*, 1957, **83**, 1401-1/1401-22.

[5] Chachereau, Y., & Chanson, H., Bubbly Flow Measurements in Hydraulic Jumps with Small Inflow Froude Numbers, *Int. J Multiphase Flow*, 2011, **37**, 555-564.

[6] Chanson, H., Bubbly Flow Structure in Hydraulic Jump, *Eur. J. Mech. B-Fluid*, 2007, **26**, 367-384.

[7] Felder, S., & Chanson, H., Phase-detection probe measurements in high-velocity free-surface flows including a discussion of key sampling parameters, *Exp. Therm. Fluid Sci.*, 2015, **61**, 66-78.

[8] Felder, S. & Chanson, H., An Experimental Study of Air-water Flows in Hydraulic Jumps with Channel Bed Roughness, *WRL Research Report 259*, 2016, 166 pages.

[9] Leng, X. & Chanson, H., Breaking Bore: Physical Observations of Roller Characteristics, *Mech. Res. Comm.*, 2015, **65**, 24-29.

[10] Leutheusser, H.J., & Schiller, E.J., Hydraulic jump in a rough channel, *Int. Water Power Dam Constr.*, 1975, **27**, 186-191.

[11] Murzyn, F., & Chanson, H., Experimental Investigation of Bubbly Flow and Turbulence in Hydraulic Jumps, *Environ. Fluid Mechanics*, 2009, **9**, 143-159.

[12] Pagliara, S. & Palermo, M., Hydraulic Jumps on Rough and Smooth Beds: Aggregate Approach for Horizontal and Adverse-sloped Beds, *J. Hydraul. Res.*, 2015, **53**, 243–252.

[13] Rajaratnam, N., Hydraulic Jumps on Rough Beds. *Trans. Eng. Inst. Canada*, 1968, **11**, 1–8.

[14] Wang, H., Turbulence and Air Entrainment in Hydraulic Jumps. *Ph.D. thesis*, 2014, School of Civil Engineering, The University of Queensland, Australia, 341 pages.

[15] Wang, H., Felder, S., & Chanson, H., An Experimental Study of Turbulent Two-Phase Flow in Hydraulic Jumps and Application of a Triple Decomposition Technique. *Exp Fluids*, 2014, **55**, Paper 1775.

[16] Zhang, W., Liu, M., Zhu, D., & Rajaratnam, N., Mean and Turbulent Bubble Velocities in Free Hydraulic Jumps for Small to Intermediate Froude Numbers. *J. Hydraul. Eng., ASCE*, 2014, **140**, paper 04014055